

# A miniature three-component LDV probe

Oleksandr Ivanchenko, Ergin Esirgemez and Semih Ölçmen

The University of Alabama, Tuscaloosa, AL 35487, USA

Received 19 January 2007, in final form 25 March 2007

Published 21 May 2007

Online at [stacks.iop.org/MST/18/2014](http://stacks.iop.org/MST/18/2014)

## Abstract

In this paper, development of a three-simultaneous-velocity component, miniature, traversable fibre-optic laser Doppler velocimetry probe head is described. The cylindrical probe head has a diameter of  $D = 12$  mm and a length of about  $L = 75$  mm. While the two velocity components perpendicular to the probe axis are measured using conventional laser-Doppler velocimetry concepts, the third component along the probe axis is measured using a heterodyne technique. The miniature probe was designed small enough to be inserted into wind-tunnel models and to fit into most common spark-plug ports to make measurements in working car engines. The probe was initially tested in a round free-jet flow to demonstrate its capabilities.

**Keywords:** turbulence, laser Doppler velocimetry

(Some figures in this article are in colour only in the electronic version)

## 1. Introduction

Measurements over models in large wind tunnels require either large focal length LDV probes to access the flow field from outside the wind tunnel (Butefisch 1989) or unique probes that can be inserted into the model. Examples of unique miniature LDV probes exist in the literature, such as the probes by Chesnakas and Simpson (1997), and by Byun *et al* (2004) for measurements on stationary models, and by Favier *et al* (1997), for measurements on rotating frames. Additionally, measurement in unique applications such as the measurements within the cylinder of working cars requires special probes to be built. Recently Bopp *et al* (1990), Ikeda *et al* (2000) and Kim *et al* (2002) have developed a non-traversable LDV probe which could fit into an M14 size spark plug to measure turbulence at the spark-plug location under motored engine conditions. Esirgemez and Ölçmen (2005) have reported a novel two-component, fibre-optic, traversable LDV probe that could fit into the most common spark-plug (size M8) ports. Reviews of the recent state-of-the-art techniques used in flow field investigation of fired production engines (Hassel and Linow 2000, Zhao and Ladommatos 1998, Kuwahara and Ando 2000, Kuwahara 2003) indicate the fact that expensive engines with special optical access are required for such research.

The present paper describes the development of a sub-miniature, traversable, fibre-optic, three-simultaneous-velocity component single-head LDV probe that can be

inserted into wind-tunnel models or into conventional car spark-plug ports. Three-simultaneous-velocity component measurements are required within a coincidence window (time window) to calculate the mean velocity, shear stress components and higher order products from the measured data. The probe can be traversed about 60 mm along the probe axis. The main difference between the current design and the previous three-dimensional LDV probe designs is that the previous designs require two separate probe heads to work together to measure the velocity components resulting in a comparatively large size probe (Byun *et al* 2004), or that the uncertainty in the velocity component measured along the probe axis is comparatively large (three-component five-beam probe offered by Dantec Inc.). The novel design described in the current paper incorporates the lessons learned from the development of the two-component probe (Esirgemez and Ölçmen 2005). In this paper first the LDV system components and the probe working principles are described. Next the experimental setup and test results obtained demonstrating the probe working principles are discussed.

## 2. LDV system

Data acquisition with an LDV system requires on-table optical equipment, a probe and the data acquisition and reduction units. In the present research, the on-table optical equipment is used to generate the four laser beams required for the velocity measurements and to couple them to fibre-optic cables that

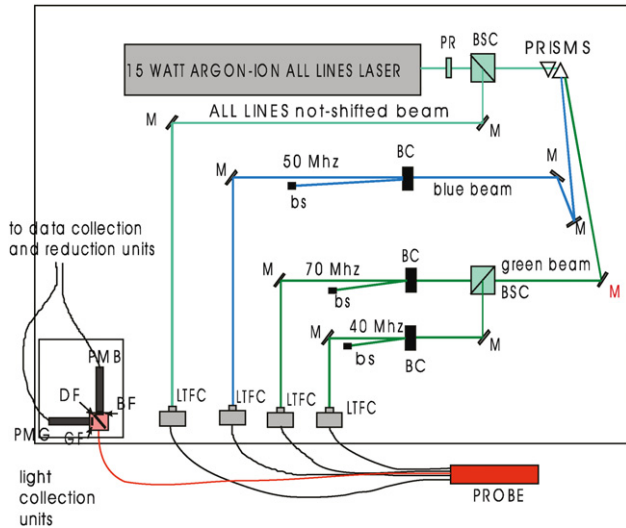


**Figure 1.** On-table optics. LTFC: laser-to-fibre coupler, M: mirror, PR: polarization rotator, BSC: beam splitter cube, PMB: photo-multiplier tube detecting blue light, PMG: photo-multiplier tube detecting green light, DF: dichroic filter, GF: green narrow band-pass filter, BF: blue band-pass filter, BC: Bragg cell, bs: beam stop.

transfer them to the probe head. The probe head is used to generate the measurement probe volumes, collect the scattered light from the particles within the flow and transfer them to the data acquisition and reduction units. The data acquisition and reduction units are used to extract the velocity information. In this section the details of each unit are briefly described.

### 2.1. On-table optics

On-table optics are used to generate the four laser beams required in the present work and couple them to the fibre-optic cables to be transmitted to the probe head (figure 1). In the current design a Spectra-Physics argon-ion laser (Beamlok-2080-15S) with a maximum output of 15W-all-lines, equipped with an etalon was used to generate two green beams (514.5 nm), one blue beam (488 nm) and another all-lines beam. While the all-lines beam was generated with the use of a polarization-rotator/beam-splitter cube couple working as a beam splitter at the exit of the laser, the rest of the all-lines laser beam was passed through two dispersion prisms working in tandem. The dispersion prisms were used to split the all-lines beam into different colour beams, and among these colours only the green and the blue beams were used. The green and the blue beams were further frequency shifted with the use of Bragg cells (Intra-Action AOM-40, AOM-50 and AOM-70) in order to eliminate the velocity directional ambiguity that would occur without such a shift. Laser beams were further coupled to fibre-optic cables (Corning® PM 48-P-S) using laser-to-fibre couplers (Newport, F-91-C1).

### 2.2. LDV Probe

The probe head unit houses transmitting and receiving fibre terminators, lenses and a beam splitter plate (figure 2), and it is responsible for generating the measurement probe volume and collecting the scattered light from the particles in the flow. The

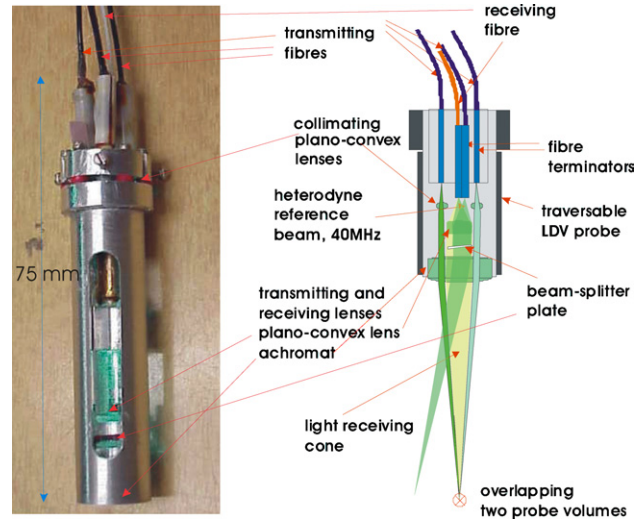


**Figure 2.** Photograph and the schematic of the LDV probe.

laser beams generated by the on-table optics are transferred to the probe head by optical fibres and the fibres are terminated separately in fibre terminators. Three of the fibre terminators were placed as if they were at the corners of an equilateral triangle. Beams emerging from the terminators pass through separate lenses for collimation. Three collimated beams next pass through a lens that focuses them to the measurement probe volume, which is the volume formed by the intersection of the beams with dimensions  $70 \mu\text{m} \times 70 \mu\text{m} \times 1337 \mu\text{m}$ . In the design, the all-lines beam (0 MHz shifted) and two green beams (70, 40 MHz shifted) were used to generate the two frequency-separated interference patterns to measure the velocity components in a plane perpendicular to the probe axis.

For measurements using the heterodyne technique an additional blue beam used as the reference beam (50 MHz shifted) was allowed to emerge from a fibre terminator that was placed right beside the receiving fibre terminator. The light scattered by the particles in the probe volume from the 0 MHz shifted all-lines laser beam together with the reference beam are used in the heterodyne technique. The heterodyne technique is described in section 3 of this paper. A beam splitter plate with reflected-to-transmitted light ratio of 10/90 was placed between the transmitting/receiving lenses to reflect the heterodyne reference beam to the receiving fibre. The reference beam passes through the plano-convex lens and becomes collimated before being reflected back from the splitter plate. The splitter plate was adjusted at a small angle (fraction of a degree) such that the light reflected back from the splitter plate passing back through the plano-convex lens could be focused on the receiving fibre terminator.

The receiving optics train is also housed in the probe head. The light scattered by the particles passing through the measurement probe volume is collected by two lenses working in tandem and is focused on the receiving optical fibre. The achromatic lens of the transmitting optics together with a plano-convex lens is used as the receiving optics to collect the scattered light from the probe volumes. A multi-mode,  $50 \mu\text{m}$  core-diameter receiving fibre is used to transfer the collected light to the data acquisition unit. Table 1 gives some of the details of the probe optical equipment.

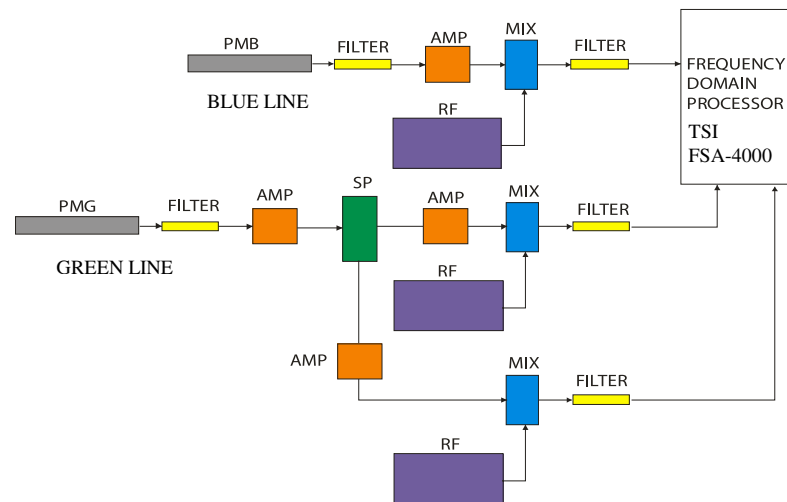


**Figure 3.** Data collection and reduction units. PMB: photo-multiplier tube for blue light; PMG: photo-multiplier tube for green light; AMP: amplifier; MIX: mixer; SP: power splitter; RF: radio-frequency generator.

**Table 1.** Probe optical specifications.

Dimension	Splitter plate	Collimating lenses	Receiving lens	Transmitting lens
Diameter (mm)	5	3	5	10
Focal length (mm)	None	3	10	60

2.3. Data acquisition and reduction units

The light collected from the probe volume transmitted back to the data acquisition and reduction units by the receiving fibre is used to extract the velocity information. The data collection and reduction units consist of the light collection unit, electronics to amplify the signal, frequency-domain processor to extract the Doppler information and a computer to collect and reduce the data (figure 3).

The light collection unit (figure 1) located on the optical table consists of a dichroic filter to separate the collected light into separate blue and green beams, two narrow-band pass optical filters to further separate each of the green and blue beams and two photo-multiplier tubes (Electron Tubes, 9124SB) to convert the light signal to an electrical signal. The electrical signals from each of the photo-multiplier tubes are next amplified (figure 3) using passive amplifiers (MiniCircuits, ZFL-1000LN) and frequency downmixed using radio-frequency generators (B&K 2005 BRF) to the frequency levels that the frequency-domain processor (TSI-FSA-4000) could accept.

The electrical signal corresponding to the blue beam is first high-pass filtered at 25 MHz to omit the low frequency content, next it is amplified and mixed with a radio frequency of about 46 MHz to downshift the frequency to an acceptable range of the frequency-domain processor. The signal is next low-pass filtered using a 10.7 MHz filter prior entering the frequency-domain processor to further clean the signal from the spurious frequency content. The green beam signal on the other was first split into two separate signals using a power splitter (MiniCircuits, ZSC-2-1) since it contains the signals both at around 40 and 70 MHz. Each leg of the signal is

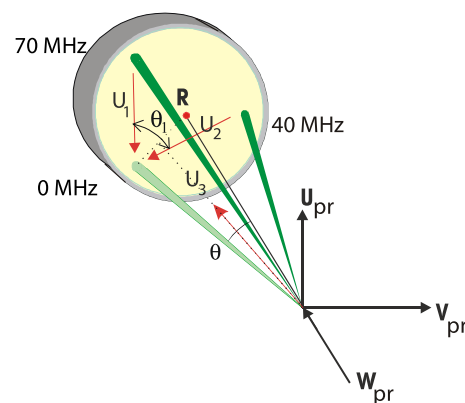


**Figure 4.** Orientation of the laser beams and velocity vectors in the probe coordinate system.

next conditioned similar to the blue beam signal prior to the frequency-domain processor.

3. Probe working principle

As mentioned earlier the probe head was developed to measure the three simultaneous velocity components at a point. While two of the velocity components perpendicular to the axis of the probe are measured using a conventional dual-beam anemometry technique (Albrecht *et al* 2003, Esirgemez and Ölçmen 2005), the third velocity component along the probe axis is measured using a heterodyne measurement technique (figure 4). In this section these techniques are briefly discussed and the geometrical relations between the measured velocity components and the fluid velocity vector components are described.

3.1. Heterodyne method

The heterodyne method was used in measuring the velocity component along the axis of the probe with the working principle directly based on the Doppler effect. The dynamic

scattering of coherent light by a moving particle causes a Doppler frequency shift,  $\Delta f_{\text{Dop}}$ , of the original light frequency,  $f_0$ , with a wavelength of  $\lambda_0$ , depending on the particle velocity vector,  $\vec{v}_p$ , the unit vector of the incident light direction  $\vec{e}_i$ , and the observer direction unit vector  $\vec{e}_r$ , resulting in a  $f_r$  frequency observed by the observer:

$$f_r = f_0 + \frac{\vec{v}_p \cdot (\vec{e}_r - \vec{e}_i)}{\lambda_0} = f_0 + \Delta f_{\text{Dop}}. \quad (1)$$

For a particle with a velocity vector,  $\vec{v}_p = v_{px} \cdot \vec{i} + v_{py} \cdot \vec{j} + v_{pz} \cdot \vec{k}$  and the unit vectors in the receiver and the incident beam directions as  $\vec{e}_r = e_{rx} \cdot \vec{i} + e_{ry} \cdot \vec{j} + e_{rz} \cdot \vec{k}$  and  $\vec{e}_i = e_{ix} \cdot \vec{i} + e_{iy} \cdot \vec{j} + e_{iz} \cdot \vec{k}$ , respectively, the Doppler frequency shift can be written as

$$\Delta f_{\text{Dop}} = (v_{px}(e_{rx} - e_{ix}) + v_{py}(e_{ry} - e_{iy}) + v_{pz}(e_{rz} - e_{iz}))/\lambda_0. \quad (2)$$

The heterodyne method uses the Doppler frequency shift,  $\Delta f_{\text{Dop}}$ , to quantify the velocity along the probe axis. To measure the  $\Delta f_{\text{Dop}}$  first the light scattered from the particles illuminated by the all-lines laser beam (0 MHz shifted beam) is interfered with the heterodyne-reference beam (50 MHz shifted beam). The interference of these beams in the air medium before the receiving optics fibre terminator transforms the Doppler frequency shift information into amplitude oscillations by phase discrimination that can be observed by the receiving optics train. In order to obtain amplitude oscillations on the fibre terminator, the angle between the scattered light and the reference beam needs to be close to zero in order to minimize fringe formation, and the receiving aperture should be larger than or equal to the size of fringe spacing on the fibre terminator. The amplitude oscillation signal is next processed in the same fashion similar to the other signals to extract the Doppler shift frequency.

### 3.2. Dual-beam anemometry

Dual-beam anemometry was used in measuring the velocity components perpendicular to the probe axis. If two laser beams are focused at the same point in the fluid the observed Doppler frequency can be expressed using equation (1) as

$$f_r = f_0 + \frac{\vec{v}_p \cdot (\vec{e}_r - \vec{e}_2)}{\lambda_0} - \left( f_0 + \frac{\vec{v}_p \cdot (\vec{e}_r - \vec{e}_1)}{\lambda_0} \right) = \frac{\vec{v}_p \cdot (\vec{e}_2 - \vec{e}_1)}{\lambda_0}, \quad (3)$$

where  $\vec{e}_1$  and  $\vec{e}_2$  are the unit vectors along each laser beam. Equation (3) shows that the observer direction unit vector  $\vec{e}_r$  is not included in the expression indicating that the observed frequency does not change with the observer direction. The interference of the laser beams with an included angle  $\alpha$  between them results in fringes with  $f_s = \frac{\lambda_0}{2 \sin(\alpha/2)}$  spacing in the measurement volume. The velocity component measured with such a system is the component perpendicular to the fringes ( $v_{p\perp} = f_s \cdot \Delta f_{\text{Dop}}$ ). In the current design three beams were used to generate frequency separated two interference patterns (between 0 and 40 MHz, and 0 and 70 MHz shifted beams) to measure the two velocity components.

### 3.3. The velocity components calculation

The velocity components  $U_1$ ,  $U_2$  and  $U_3$  measured by the probe shown in figure 4 were first used to calculate the  $U_{pr}$ ,  $V_{pr}$ ,  $W_{pr}$  velocity components in a coordinate system attached to the probe. The  $U_{pr}$  and  $V_{pr}$  velocity components in a plane perpendicular to the probe axis are calculated using the relations:

$$U_{pr} = -U_1, \quad V_{pr} = (U_2 + U_{pr} \cos(\theta_1))/\sin(\theta_1) \quad (4)$$

where  $U_1 = \Delta f_{\text{Dop}1} \cdot \lambda_g / (2 \sin(\alpha/2))$  and  $U_2 = \Delta f_{\text{Dop}2} \cdot \lambda_g / (2 \sin(\alpha/2))$  are the velocity components measured,  $\theta_1$  is the angle between the two velocity components and  $\lambda_g = 514.5$  nm. The angle  $\theta_1$  is calculated by using geometry and by measuring the distances between the beams emerging from the probe head at a distant wall parallel to the probe front surface.

In the probe coordinate system the unit vectors along the transmitting and receiving directions can be written as

$$\vec{e}_r = \vec{k}_{pr},$$

$$\vec{e}_i = \cos(\theta_1/2) \sin(\theta) \cdot \vec{i}_{pr} + \sin(\theta_1/2) \sin(\theta) \cdot \vec{j}_{pr} - \cos(\theta) \cdot \vec{k}_{pr}.$$

Using the  $U_3$  expression,  $U_3 = \Delta f_{\text{Dop}3} \cdot \lambda_b / (2 \cos^2(\theta/2))$  calculated by employing equation (2), the axial velocity component,  $W_{pr}$ , can be written as

$$W_{pr} = U_3 + (V_{pr} \sin(\theta_1/2) + U_{pr} \cos(\theta_1/2)) \tan(\theta/2), \quad (5)$$

where  $\lambda_b = 488$  nm.

The expressions for the  $U_1$ ,  $U_2$  and  $U_3$  velocity components can also be used to estimate the sensitivity,  $\text{Sn}$  ( $\text{Sn}_i$  = the Doppler frequency shift that a  $1 \text{ m s}^{-1}$  flow velocity results) of the heterodyne method and the dual-beam anemometry method. With the knowledge of the wavelengths for the laser beams and with  $\theta \approx 4^\circ$ ,  $\alpha \approx 6^\circ$ , the sensitivities can be calculated as  $\text{Sn}_1 = \text{Sn}_2 \approx 0.2 \text{ MHz}/(\text{m s}^{-1})$  for the dual-beam anemometry method and,  $\text{Sn}_3 \approx 4 \text{ MHz}/(\text{m s}^{-1})$  for the heterodyne method. The increase in the sensitivity along the probe axis presents a unique characteristic of the probe design. The probe would be most suitable for measurements of small velocity components with 20 times resolution of the dual-beam method.

## 4. Experiments: setup, data reduction equations and results

### 4.1. Experimental setup

The probe developed was next tested in a well-defined air-jet flow to demonstrate the working principles of the probe. The jet flow for this experiment was produced by a hot-wire anemometry calibrator (TSI Model 1125) (figure 5(A)). The calibrator exit free jet velocity was measured by means of an inclined manometer using Bernoulli's equation. A schematic of the axisymmetric free-jet flow studied, and the coordinate systems used in the study are shown in figure 5(B). The velocity components in  $x$ ,  $r$  and  $\theta$  coordinate directions are  $U$ ,  $V$ ,  $W$ , respectively. The Reynolds number for the jet, based on the jet diameter ( $d = 3.81$  mm,  $R = d/2$ ) and exit velocity was allowed to vary between  $Re_D = 3914$  and  $9134$  resulting in the turbulent jet. Di-octyl-phthalate seeding particles with a mean

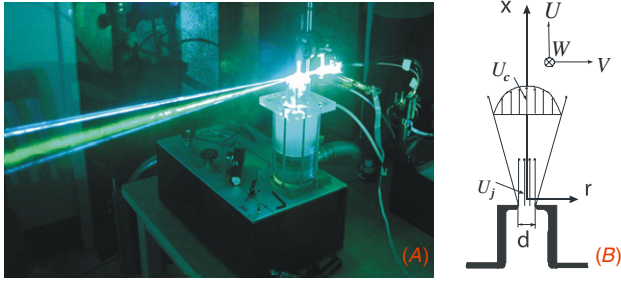


Figure 5. Experimental setup.

diameter of  $0.7 \mu\text{m}$  generated by a six-jet atomizer (TSI-9306) were introduced into the calibrator-settling chamber to seed the flow.

The LDV probe was held by a traversing mechanism, which provided the movement in the radial direction. Sliding the probe holder up and down, allowed the distance from the jet flow exit to be changed. The velocity measurements were made at the jet exit about  $0.25d$  above the exit plane. The velocity components measured in the probe coordinate system were further transformed to the jet coordinate system.

#### 4.2. Experimental results

The following experiments were performed to demonstrate that the probe worked as designed:

*Test 1.* Jet-exit velocity and turbulence profiles were obtained as the probe was traversed in the radial direction along a diameter of the jet at  $0^\circ$  and  $10^\circ$  angular orientations of the probe with respect to the jet-exit surface plane ( $U_j = 24 \text{ m s}^{-1}$ ).

*Test 2.* Velocity and turbulence measurements were performed at different angular orientations of the probe at a known jet-exit velocity at the jet centre at the exit plane ( $U_j = 24 \text{ m s}^{-1}$ ).

*Test 3.* Velocity and turbulence measurements at  $10^\circ$  orientation of the probe were made at pre-selected multiple jet mean velocity values at the jet centre at the exit plane.

The mean velocities, normal stresses and the Reynolds stress were calculated using the particle residence time as the weighting factor to eliminate the bias due to particle-rate/velocity correlation that may exist during the measurements (Albrecht *et al* 2003, Edwards 1987). The residence time is the time the particle spends in the probe volume as given by the frequency-domain processors for each valid signal, and it is also named the ‘gate pulse’ as discussed in section 6.2 in Albrecht *et al* (2003). Prior to the residence time averaging, velocity data were first used to calculate the standard deviation,  $\sigma$ , of the data. Next the data outside  $\pm 3\sigma$  were discarded. Three-component simultaneous velocity measurements were obtained within a  $10 \mu\text{s}$  coincidence interval to obtain coincident data required in calculating fluctuating velocity products. At most measurement locations 25 000 data points were recorded, with a sampling rate of  $2000 \text{ samples s}^{-1}$ . The mean velocity, turbulence fluctuating velocity, Reynolds stresses were calculated using the following equations:

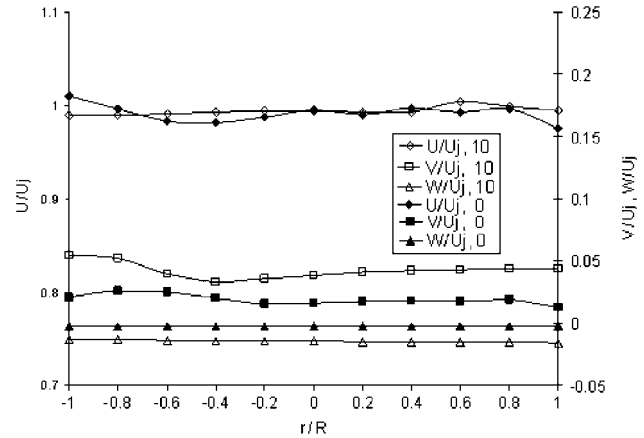


Figure 6. Jet-exit mean velocity profiles at  $0^\circ$  and  $10^\circ$  probe orientations.

$$\bar{V} = \frac{\sum_{i=1}^N V_i \cdot \Delta t_i}{\sum_{i=1}^N \Delta t_i} \quad (6)$$

$$v = \sqrt{\frac{\sum_{i=1}^N (V_i - \bar{V})^2 \cdot \Delta t_i}{\sum_{i=1}^N \Delta t_i}} \quad (7)$$

$$\overline{uv} = \frac{\sum_{i=1}^N (V_i - \bar{V})(U_i - \bar{U}) \cdot \Delta t_i}{\sum_{i=1}^N \Delta t_i}, \quad (8)$$

where  $\bar{V}$  is the mean velocity,  $V_i$  is the recorded velocity,  $\Delta t_i$  is the length of time a particle spends in the measurement volume as detected by the frequency-domain processor and  $N$  is the number of data points.

*Test 1.* Mean velocity profiles non-dimensionalized using the jet-exit velocity,  $U_j = 24 \text{ m s}^{-1}$ , obtained at the jet exit at  $0^\circ$  and  $10^\circ$  probe orientations are shown in figure 6. Profiles show that near the exit, the axial velocity of the jet has a ‘top-hat’ profile, in which the velocity is constant across the width of the jet, until it decreases rapidly at the edges. The velocity at the jet exit is uniform and radial and the tangential velocity components are close to zero. Profiles obtained with the two different probe orientations show that the  $U/U_j$  values differ  $\sim 1.5\%$  from each other with the largest difference being  $\sim 2.5\%$ , while the  $V/U_j$  and  $W/U_j$  values differ from each other by  $\sim 2\%$  and  $\sim 4\%$ , respectively. The plots of the turbulent fluctuating velocity components at the jet exit at  $0^\circ$  and  $10^\circ$  probe orientations are shown in figure 7. The differences between the fluctuating velocity components obtained with different probe orientations are  $\sim 1\%$  of the mean jet velocity with  $\sim 1.5\%$  largest difference. Both figures indicate that mean velocity and the turbulence quantities measured at different probe orientations are close to each other as expected.

*Test 2.* As another test the flow velocity at the centre of the jet exit was measured with different angular positions of the probe. The probe angular orientation was changed from  $0^\circ$  to  $60^\circ$  with respect to the jet-exit surface plane while the jet-exit velocity was kept as  $U_j = 24 \text{ m s}^{-1}$ . The results of these experiments are shown in figure 8. As the probe was rotated

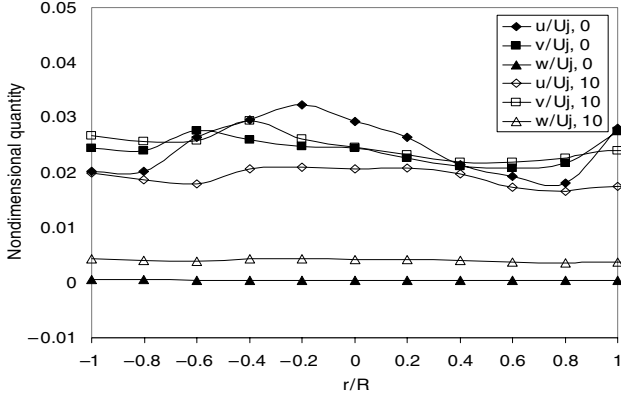


**Figure 7.** Jet-exit fluctuating velocity profiles at  $0^\circ$  and  $10^\circ$  probe positions.

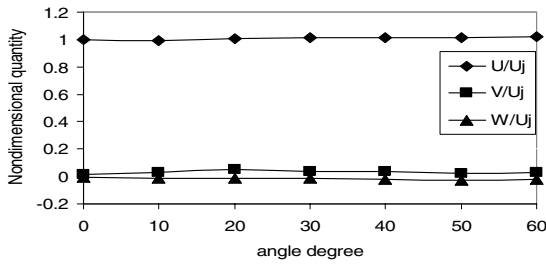


**Figure 8.** Mean velocity values obtained at different probe angular orientations,  $U_j = 24 \text{ m s}^{-1}$  at the centre of the jet exit.

around the horizontal  $y$ -axis by an angle  $\beta$ , the  $V$  component of velocity measured by the probe did not change with respect to the jet coordinate system. The other velocity components measured in the probe coordinate system were transformed to the jet coordinate system.

The results agree closely with the results for the zero angular position. The largest differences between the  $U$ ,  $V$  and  $W$  component data obtained at  $0^\circ$  and at other angles are about 2% of the mean jet velocity. The differences between the data are within the uncertainty bands including the uncertainty of the angular and the axial positions of the probe with respect to the jet, indicating that the probe can be used at any chosen orientation.

*Test 3.* The last set of experiments was made once the probe was held at  $10^\circ$  angular orientation at different preset jet mean velocity values resulting in different Reynolds numbers of the jet (figures 9 and 10). The  $U$  velocity component data are very close to the expected results ( $U/U_j = 1$ ) with the measured velocity values within 2% of the preset velocity. The largest difference was observed at  $U_j = 15 \text{ m s}^{-1}$  with a 4% difference. The fluctuating velocity data indicate that the  $u/U_j$  and  $\overline{uv}/U_j^2$  values increase with increasing Reynolds number similar to the observations by Kwon and Seo (2005).

## 5. Uncertainty analysis

Data uncertainties were determined using two separate data sets and using Chauvenet's criterion (Holman 1978). For this purpose two profiles taken at the jet exit at  $10^\circ$  and  $0^\circ$  probe

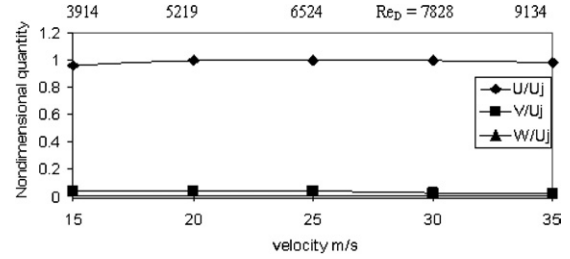


**Figure 9.** Mean velocity values obtained at  $10^\circ$  probe angular orientation at different jet-exit velocities at the centre of the jet exit.

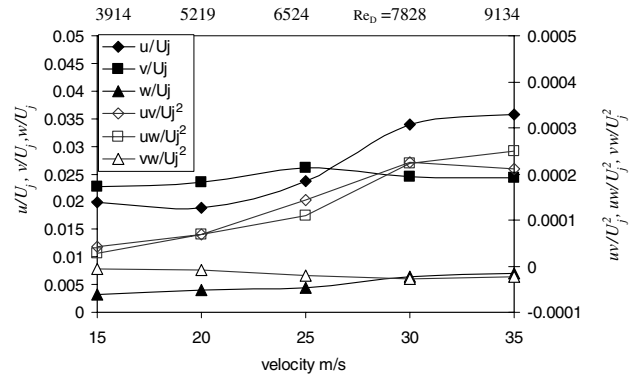


**Figure 10.** Fluctuating velocity and kinematic shear stress obtained at  $10^\circ$  probe angular orientation at different jet-exit velocities at the centre of the jet exit.

**Table 2.** Uncertainties ( $\pm 2\sigma$ ) in measured quantities at 21:1 odds.

Velocity component	$U/U_j$	$V \text{ (m s}^{-1}\text{)}$	$W \text{ (m s}^{-1}\text{)}$
Uncertainty	$\pm 0.012$	$\pm 0.5$	$\pm 0.55$

angular orientations under the same jet-exit conditions were used ( $U_j = 24 \text{ m s}^{-1}$ ). The velocity components were first determined in the jet coordinate system in order to express the data in a single coordinate system and also to include the effect of coordinate transformation in the uncertainty analysis. The data were used to calculate the average of half of the absolute differences between two data values for each quantity to determine the  $d_{\max}$ . The standard deviation,  $\sigma$ , was calculated using

$$\frac{d_{\max}}{\sigma} = 1.15. \quad (9)$$

The uncertainties presented in table 2 are for  $2\sigma$  deviation, which results in 21:1 odds that repeat measurements will fall within this deviation. The  $U$  velocity component is non-dimensionalized by the centreline axial velocity, while for the  $V$  and the  $W$ , the uncertainties were expressed in  $\text{m s}^{-1}$  since the measured velocity components were very close to zero thus indicating the velocity resolution of the probe perpendicular to the probe axis.

## 6. Conclusions

In this paper the design and testing of a unique miniature fibre-optic 3D probe is described. The 3D-LDV probe

was designed to measure the three components of the velocity simultaneously using the dual-beam method and heterodyne measurement techniques. The probe was built and tested in a round free-jet flow. It was shown in the body of the paper that the probe permits measurement of three components of the flow velocity simultaneously to deduce the three mean and three fluctuating components of velocity as well as the higher order products. The probe was tested at different angular positions and different jet-exit velocities. The measurements showed that the differences between preset and measured velocity were less than 2%. The high sensitivity of the probe for the measurement of the axial velocity presents an additional unique capability of the probe. This allows for very small velocity magnitude measurements, such as the vertical component of the velocity in a boundary layer.

### Acknowledgments

This work was supported by the Center for Advanced Vehicle Technologies (CAVT) of the University of Alabama. The authors would like to thank Dr Clark Midkiff for his support and encouragement.

### References

- Albrecht H E, Borys M, Damaschke N and Tropea C 2003 *Laser Doppler and Phase Doppler Measurement Techniques* (Berlin: Springer)
- Bopp S, Durst F and Tropea C 1990 In-cylinder velocity measurements with a mobile fiber optic LDV system *SAE Paper*, 900055.
- Butefisch K A 1989 Three component laser Doppler anemometry in large wind tunnels *Prog. Aerospace Sci.* **26** 79–113
- Byun G, Ölçmen M S and Simpson R L 2004 A three-velocity-component sub-miniature laser-Doppler velocimeter for measurements of a turbulent boundary layer *Meas. Sci. Technol.* **15** 2075–82
- Chesnakas C J and Simpson R L 1997 Detailed investigation of the three-dimensional separation about a 6:1 prolate spheroid *AIAA J.* **35** 990–9
- Dantec Inc., <http://www.dantecdynamics.com/Default.aspx?ID=690>
- Edwards R V 1987 Report of the special panel on statistical particle bias problems in laser anemometry *Trans. ASME, J. Fluids Eng.* **109** 89–93
- Esirgomez E and Ölçmen M S 2005 Spark-plug LDV probe for in-cylinder flow analysis of production IC engines *Meas. Sci. Technol.* **16** 2038–47
- Favier D, Maresca C, Nsi Mba M, Berton E and Agnes A 1997 New type of embedded laser Doppler velocimeter for measurement of rotary wings boundary layer *Rev. Sci. Instrum.* **68** 2247–55
- Hassel E P and Linow S 2000 Laser diagnostics for studies of turbulent combustion *Meas. Sci. Technol.* **11** R37–R57
- Holman J P 1978 *Experimental Methods for Engineers* (New York: McGraw-Hill)
- Ikeda Y, Nishihara H and Nakajima T 2000 Spark plug-in fiber LDV for turbulent intensity measurement of practical SI engine *10th Int. Symp. on Applications of Laser Techniques to Fluid Mechanics (Lisbon, Portugal, 10–13 July)*
- Kim B, Kaneko M, Mitani M, Ikeda Y and Nakajima 2002 In-cylinder turbulent measurements with a spark plug-in fibre LDV *11th Symposia on Applications of Laser Techniques to Fluid Mechanics (Lisbon, Portugal, 8–11 July)*
- Kuwahara K 2003 In-cylinder phenomena diagnostics for gasoline engine development *Tech. Rev.* **15** 21–31
- Kuwahara K and Ando H 2000 Diagnostics of in-cylinder flow, mixing and combustion in gasoline engines *Meas. Sci. Technol.* **11** R95–R111
- Kwon S J and Seo I W 2005 Reynolds number effects on the behavior of a non-buoyant round jet *Exp. Fluids* **38** 801–12
- Zhao H and Ladommatos N 1998 Optical diagnostics for in-cylinder mixture formation measurements in IC engines *Prog. Energy Combust. Sci.* **24** 297–36